

panel serves as an effective solution for temporary structural construction [12]. Shear connection tests on GFRP pultruded profiles with bolted connections to RC slabs showed an increase in both their strength and stiffness above simple GFRP profiles [13].

Nowadays, in concrete structures, GFRP bars have become an alternative to steel bars as they have high resistance to corrosion and low repair and maintenance costs [14]. This GFRP bar has higher tensile strength and is lighter in weight than steel bars [15,16]. The usage of GFRP bars for internal reinforcement of concrete structures was successfully demonstrated in many research projects examining slabs [17], beams [18], and columns [19]. Utilization of ordinary Portland cement by the construction industry results in 7% annual emissions of global CO₂. The research focused on creating low-carbon cement for the cement industry [20-23] while also exploring CO₂ curing of concrete [24-27] together with dry ice utilization as a different carbon dioxide form in concrete. The compressive strength at 28 days increased by 31% when 0.9 % dry ice by weight of cement was added to concrete, and beyond 0.9 % weight, it dropped notably [28]. Concrete benefits from the addition of GGBS, which is a steel industry residue that serves as a cement replacement. At an early age, the addition of GGBS in concrete lowers the compressive strength, and it increases at a later age. Geopolymer concrete obtained superior compressive strength by 18% using CO₂-milled slag compared to air-milled slag [29]. Moreover, the flexural strength of concrete increased when cement was replaced by GGBS up to 50% [30-38]. Additionally, GGBS-based concrete presented improved workability as the GGBS substitution level was increased [39]. Addition of GGBS reduced thermal cracking, permeability, shrinkage and creep [40-42]. The decrease in strength by the addition of GGBS could be increased with the addition of 10% micro silica [43].

Literature studies on GFRP beams and columns infilled with concrete are available. But literature pertaining to infilled GFRP 3D frames with composite GFRP deck profiles is limited. In the proposed study, two 3D frames with GFRP square sections and a GFRP- concrete

composite deck slab were investigated for their flexural behaviour. In one frame, the beams and columns were made with hollow square GFRP sections, and in the other, they were infilled with M20 grade GGBS-based concrete.

2. Materials and Methods

2.1. GGBS-Based Concrete

M20 grade sustainable concrete was used for infilling the square sections and the concrete topping of the deck, with the concrete mix formulated in accordance with IS 10262:2019 and IS 456:2000 standards. The concrete mix incorporated 53-grade OPC with 60% GGBS [34] substitution along with M-sand as fine aggregate. The size of coarse aggregate is 10mm and 20mm gravel, 10% micro silica [43], 0.9% CO₂ dry ice [28], and 3% self-curing agent (Polyethylene-Glycol). Replacing 60% of OPC with GGBS results in significant CO₂ savings, because GGBS production emits far less carbon compared to OPC. To enhance durability and compensate for the reduction in early strength caused by the 60% replacement of cement with GGBS, 10% micro silica was incorporated into the concrete mix.

For infilling the square sections with sustainable concrete, the M20 grade mix incorporated 10mm M-sand as the coarse aggregate while retaining the other ingredients unchanged. Table 1 displays the chemical composition of GGBS and cement. The properties of coarse aggregate and fine aggregate appear in Table 2. The mix proportions of the GGBS-based concrete containing 20 mm aggregate and 10 mm aggregate are presented in Tables 3 and 4.

In a concrete mixer, cement along with GGBS as well as micro silica, combined with M-sand and coarse aggregate to the required measurement levels, was mixed thoroughly. Then, CO₂ was added to the required levels in the form of crumbled dry ice while a lid covered the mixer opening to mix everything thoroughly for 5 additional minutes. Finally, water and self-curing agent were added to the mixer and mixed thoroughly.

Table 1. Chemical Composition of GGBS and Cement

Chemical composition (%by mass)	CaO	SiO ₂	Al ₂ O ₃	MgO	Fe ₂ O ₃	Na ₂ O	Cl	SO ₃
GGBS	34.68	33.11	21.95	1.28	-	-	-	0.1
Cement	63.2	21.06	5.72	1.9	4.38	0.25	0.01	0.4

Table 2. Properties of Course and Fine Aggregates

Test	Coarse Aggregate	Fine Aggregate
Zone/Type	Crushed granular	II
Water Absorption	0.735%	1.036%
Fineness Modulus	6.27	2.51
Specific Gravity	2.70	2.64

Table 3. Mix Proportion of GGBS-based concrete with 20mm aggregate

Water/ Binder ratio	Cement (kg/m ³)	GGBS (kg/m ³)	Coarse Aggregate (kg/m ³)	Fine Aggregate (kg/m ³)	Micro silica (kg/m ³)	Dry Ice (kg/m ³)
0.5	151	225	1169	693	37.6	1.134

Table 4. Mix Proportion of GGBS-based concrete with 10mm aggregate

Water/ Binder ratio	Cement (kg/m ³)	GGBS (kg/m ³)	Coarse Aggregate (kg/m ³)	Fine Aggregate (kg/m ³)	Micro silica (kg/m ³)	Dry Ice (kg/m ³)
0.5	168	252	893	864	42	3.78

2.2. GFRP Square Sections

GFRP hollow square sections of size 10cm x 10cm x 0.5cm were used for the beams and columns of the GFRP frame. Figure 1 shows the hollow square sections used for the beams and columns. GFRP sheet profiles of size 1200 X 900 mm and with trapezoidal cross section of 120X35x3 mm as shown in Figure 2 were used as deck slab. The fabricated GFRP sheet profile is shown in Figure 3.

**Figure 1.** Photograph of hollow GFRP square section**Figure 2.** Cross Section of GFRP Sheet Profile**Figure 3.** Fabricated GFRP sheet profile

2.3. Fabrication of 3D GFRP Frame with Concrete Composite Slab

Two, three-dimensional (3D) frame specimens were fabricated with beams and columns using Glass Fiber Reinforced Polymer (GFRP) square hollow sections and integrated with a GFRP-concrete composite deck. Each frame had overall dimensions of 1.2 m (length) × 0.9 m (width) × 1.0 m (height). The longitudinal beams were fabricated from GFRP square sections with a cross-section of 100 mm × 100 mm, thickness of 5 mm, and length of 1.0 m. The transverse beams shared the same cross-section and thickness but were 0.7 m in length. In one of the frames, the hollow sections of the beams and columns were infilled with M20 grade GGBS-based concrete to investigate the influence of concrete infill on the structural performance.

Beam-to-column connections were established using 125 mm × 100 mm × 5 mm steel angle plates, fastened with 8 mm diameter through bolts to ensure adequate rigidity and structural continuity. The trapezoidal corrugated GFRP-concrete deck slab was seated atop the beam framework and connected using 125 mm × 100 mm × 5 mm steel angle plates with 8 mm diameter through bolts at the beam-column joint and with an additional plate of size 100x100x5 mm at the centre of the longitudinal and transverse beams using the same 8mm diameter through bolts.

For slab reinforcement, 8 mm diameter GFRP rods of 225 mm (c/c) spacing along the shorter span and 240 mm (c/c) in the longer span. The 'T'-shaped shear connectors, fabricated from 8 mm GFRP rods in a spacing of 200 mm as per IS: 11384. 8 mm GFRP rods at 225 mm (c/c) for the shorter span and 240 mm (c/c) for the longer span reinforced the slabs to manage temperature and shrinkage effects. A schematic view of the 3D hollow frame with connection is shown in Figure 4, and with deck slab is shown in Figure 5. Fabricated hollow and infilled 3D frame with GFRP deck profile is shown in Figures 6, 7, whereas Figures 8, 9 depict the hollow frame and infilled frame with concrete topping, respectively. The information about the tested specimen appears in Table 5.

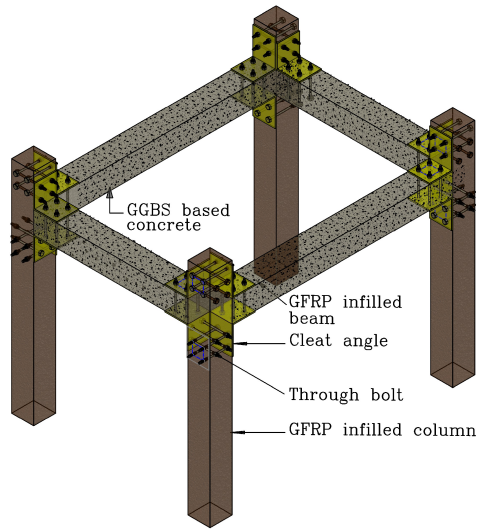


Figure 4. Schematic view of the 3D hollow frame with connection

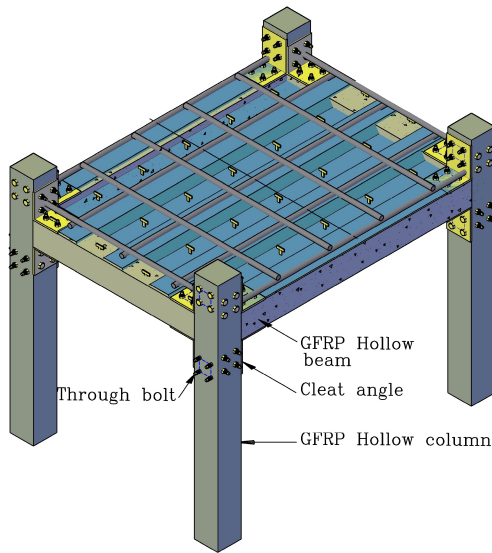


Figure 5. Schematic view of the 3D frame with GFRP deck slab

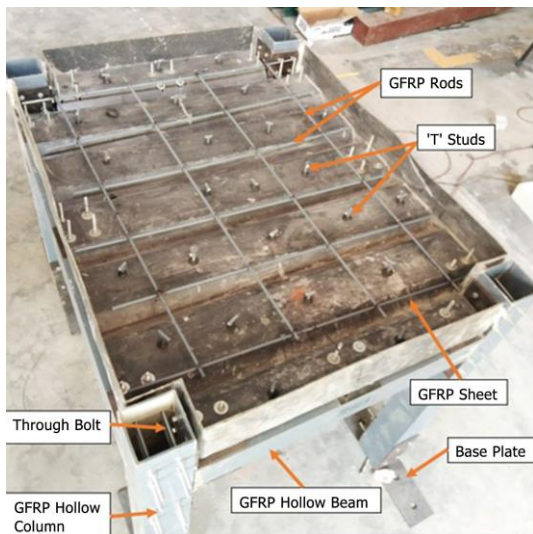


Figure 6. Fabricated hollow 3D frame with GFRP deck profile

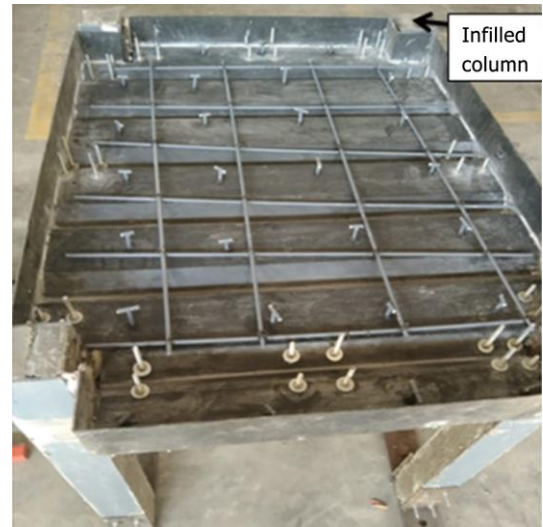


Figure 7. Fabricated infilled 3D frame with GFRP deck profile

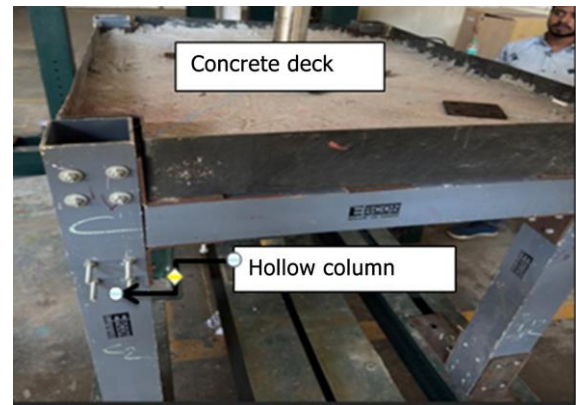


Figure 8. Fabricated hollow 3D frame with composite deck slab

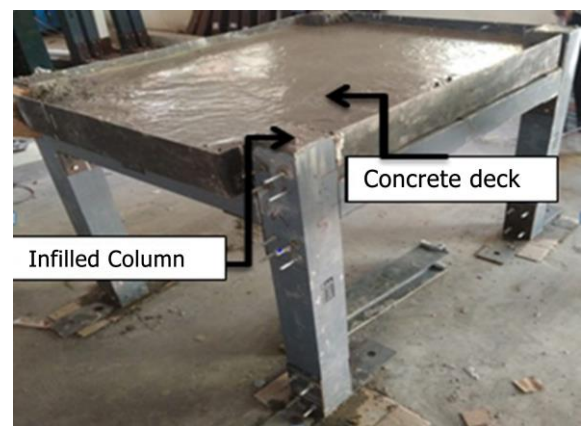


Figure 9. Fabricated infilled 3D frame with composite deck slab

Table 5. First crack load and ultimate load of hollow and infilled frames

Specimen ID	First crack load (kN)	Ultimate load (kN)
FSH (hollow)	13.7	24.82
FSI (infilled)	29.7	50.3

The specimens tested included two types: FSH and FSI. Note: The first letter denotes the frame, the second letter denotes the Square Section, and the third letter indicates whether the Beam and Column Sections are Hollow or Infilled. For the FSH specimen, the beams and columns were hollow with a beam size of $1 \times 0.1 \times 0.1 \times 0.005\text{m}$ and a column size of $0.7 \times 0.1 \times 0.1 \times 0.005\text{m}$; the deck slab incorporated a GFRP profile with a longitudinal dimension of 1.2m and a transverse dimension of 0.9m with 0.06m-thick concrete topping. For the FSI specimen, the beams and columns were infilled with the same beam size of $1 \times 0.1 \times 0.1 \times 0.005\text{m}$ and column size of $0.7 \times 0.1 \times 0.1 \times 0.005\text{m}$; the deck slab had a GFRP profile as that of FSH with a concrete topping of $1.2 \times 0.9 \times 0.06\text{m}$.

2.4. Experimental Set-up

The 3D GFRP frames were kept in a loading frame with a capacity of 40T for testing. The GFRP frames were connected to the loading frame through a base plate of size $125 \text{ mm} \times 125 \text{ mm} \times 5 \text{ mm}$ connected to the bottom of the column and with long bolts of 10mm diameter. Static Point loads were applied to the slab specimen through the load cell. The deflections of structural elements are checked with dial gauges, one at the middle of the slab and one at the center of the longitudinal beam. The 2kN/min increment load was applied to the specimen till the failure. The experimental set-up for testing the hollow and infilled frames is shown in Figure 10 and Figure 11, respectively.



Figure 10. Test set-up of hollow frame

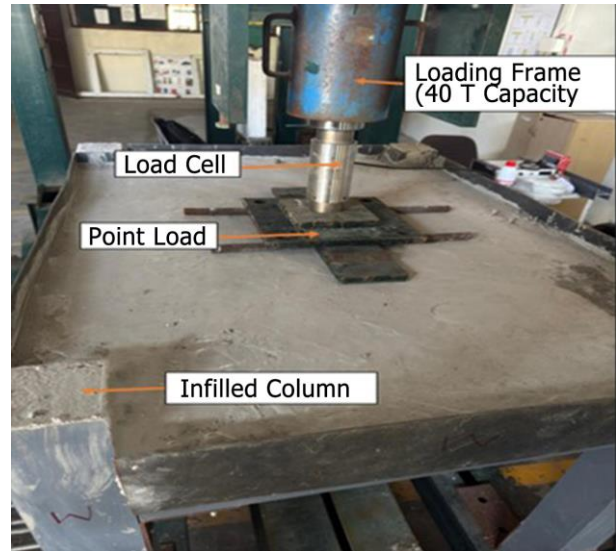


Figure 11. Test set-up of infilled frame

3. Result and Discussion

3.1. Crack Pattern

The crack pattern of the hollow and infilled frames is shown in Figures 12 and 13, respectively. The first crack load for the hollow and infilled composite frame specimens was 13.7kN and 29.7kN, respectively, as shown in Table 5. The first crack was initiated on both sides of the load at the center in the longitudinal direction, and it propagated towards the edges in the transverse direction; meanwhile, small cracks were developed very close to the loading point at the ultimate load level. Small cracks were also developed at the bottom of the GFRP sheet profile in the hollow frame. The 3D frame incorporating a hollow GFRP beam and column behaved more like a thin-walled FRP section with low flexural rigidity, which resulted in the formation of cracks at the bottom of the GFRP sheet profile. The infilled GFRP frame also failed in a similar manner, except that no crack was noticed at the bottom of the GFRP sheet profile. This behavior may be due to the improved dispersion of the load from the slab through the composite action of the concrete-GFRP interface in the infilled beams and columns, which prevented the formation of a crack at the bottom of the corrugated GFRP slab.



Figure 12. Crack Patterns a) Bottom of the slab, b) Top of the slab



Figure 13. Crack Pattern of Infilled Composite Frame

3.2. Load–Deflection Behavior of GFRP Frames

The load–deflection behaviors of beams and slabs in the hollow and infilled frames are shown in Figures 14(a-b) and 15(a-b), respectively. The ultimate load for the hollow and infilled composite frame specimens was 24.82kN and 50.3kN, respectively, as shown in Table 5. Thus, the load-carrying capacity was doubled when the beams and the columns of the frame were infilled with GGBS-based concrete. This increase can be attributed to the confinement effect provided by infilled concrete, which delayed the onset of crack formation. The deflection in the slab of the hollow frame (FSH) and the infilled frame (FSI) at ultimate load was 37.52 mm and 37.6 mm, respectively, while the longitudinal beam showed deflections of 4.52 mm and 9.1 mm

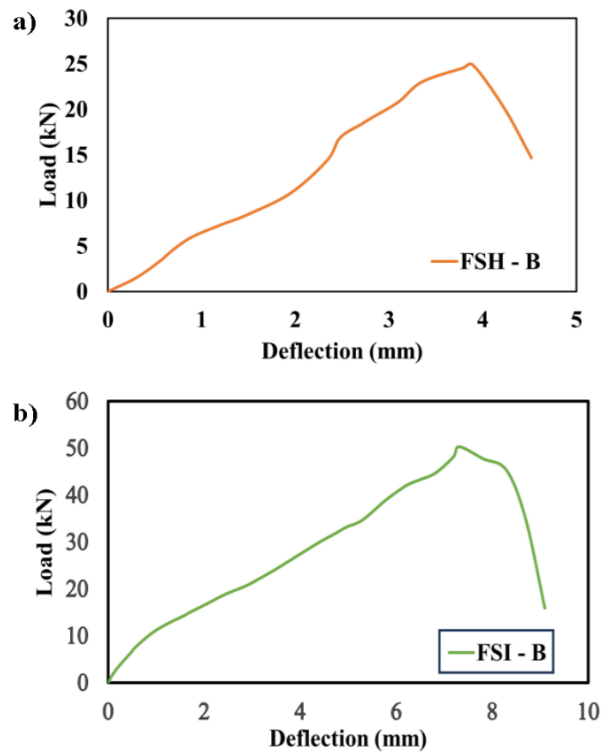
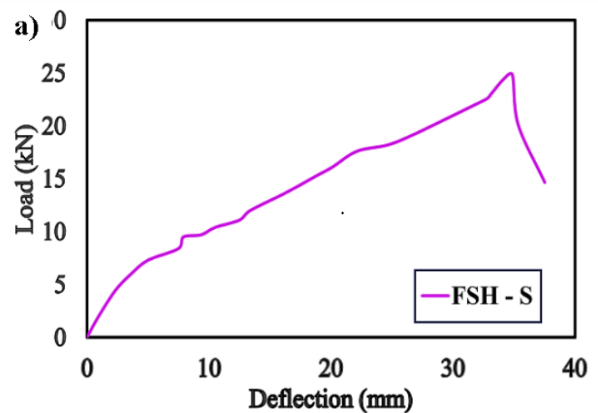


Figure 14. Load-Deflection Curves of beams in GFRP Frame



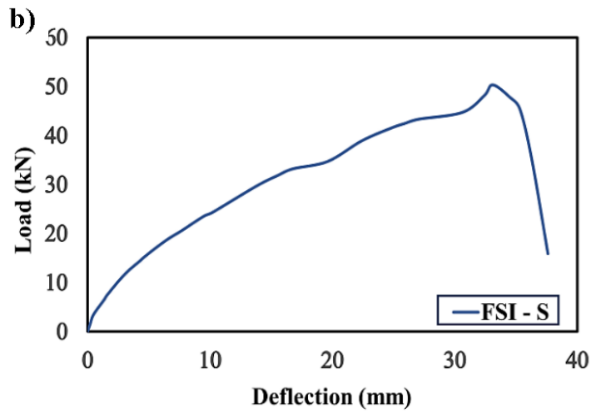


Figure 15. Load- Deflection curves of slab in GFRP Frame

The comparison of the load-deflection curves of the beams and slabs of the hollow and infilled frames is shown in Figure 16(a-d). The comparison of the load at ultimate load for the FSH and FSI is shown in Figure 17, and the comparison of deflections of the slabs and beams of the FSH and FSI is shown in Figure 18. The ultimate load-carrying capacity of the 3D GFRP frame achieved 102% increase, through infilling its beam and column sections with GGBS-based concrete. The ultimate load and deflection of the beams of the frame, incorporating infilled beams and columns, were almost 2 times more than the hollow frame, which could be due to the confinement effect provided by concrete on GFRP sections, leading to equal stiffness in both the beams of the frames. The stiffness (load-to-deflection ratio) of the beam in the infilled frame at ultimate load was 5.53 kN/mm, which was slightly higher than that of the beam in the hollow frame (5.49 kN/mm), indicating that the infilling of the GFRP beams contributes marginally to flexural stiffness, despite the increased deflection [44]. The ultimate load and deflection of the frame with infilled beams and columns are almost 2 times more than the frame with hollow beams and columns. The stiffness (load-to-deflection ratio) of the slab in the infilled frame at ultimate load was 1.33 kN/mm, which was approximately double that of the slab (0.661 kN/mm) in the hollow frame, demonstrating the significant contribution of the infill material in the beams and columns of the frame. Although the final deflection of the slabs is similar in both frames, the stiffness of the infilled frame nearly doubled because the infilled beams and columns provided much stiffer boundary support, which in turn increased the ultimate load capacity by two times. It could also be noticed that the deflection in the slab (37.2 mm) was significantly higher compared to the beam (4.52 mm), at the ultimate load in the hollow frame. A similar thing was noticed in the infilled frame also. The overall performance details of the FSH and FSI are shown in Table 6.

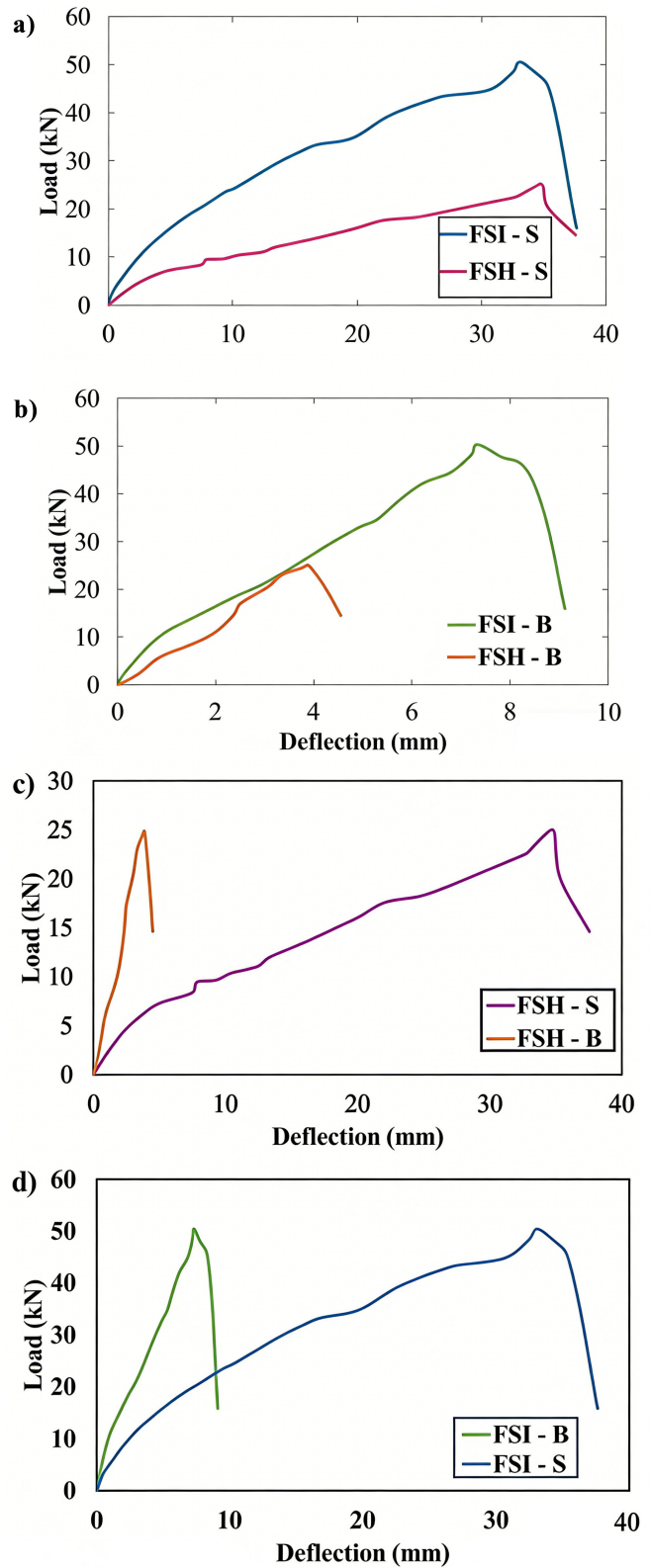


Figure 16. Comparison of load- Deflection curves of beams and slabs a) Slabs (Hollow and infilled frames), b) Beams (Hollow and infilled frames), c) Hollow frame (slab and beam), d) Infilled frame (slab and beam).

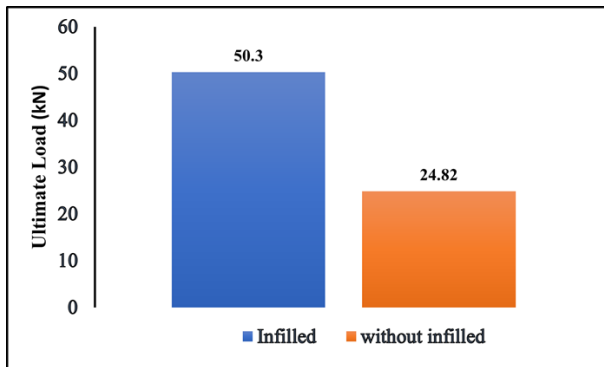


Figure 17. Comparison of the ultimate load of frames

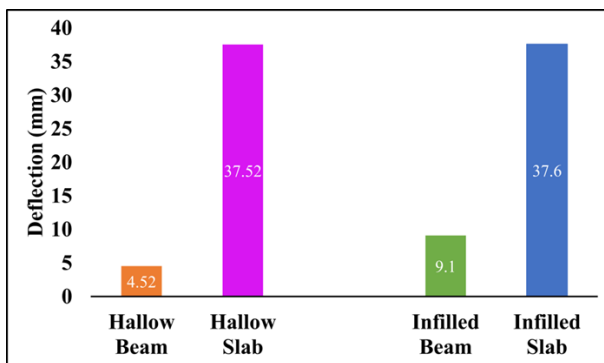


Figure 18. Comparison of deflection of the beam and slab in FSH and FSI

Table 6. Performance details of the 3D GFRP hollow and infilled frames

Specimen ID	First crack load (kN)	Ultimate load (kN)	Deflection at ultimate load (mm)	
			Beam	Slab
FSH (hollow)	13.7	24.82	4.52	37.52
FSI (infilled)	29.7	50.3	9.1	37.6

4. Conclusions

3D frames with GFRP square sections with and without infill were tested, and the following conclusions were drawn:

- The hollow GFRP frame failed due to the formation of cracks in the concrete topping, with small cracks developed at the bottom of the GFRP sheet profile. But in the Infilled GFRP frame, no crack was noticed in the GFRP deck profile.
- The 3D GFRP frame achieved 102% increase in ultimate load-carrying capacity by infilling its beam and column sections with GGBS-based concrete.
- The stiffness (load-to-deflection ratio) of the beam in the infilled frame at ultimate load was slightly higher than that of the beam in the hollow frame, indicating that the infill contributes marginally to flexural

stiffness, despite the increased deflection due to additional self-weight.

- The stiffness of the slab in the infilled frame at ultimate load was approximately double that of the slab in the hollow frame, demonstrating the significant contribution of the infill material in the beams and columns of the frame.
- It could also be noticed that the deflection in the slab was significantly higher compared to the beam at the ultimate load in the hollow and infilled frame.

Thus, infilling the beam and column sections of the GFRP frames with GGBS-based concrete significantly enhances load-carrying capacity and stiffness, making the GFRP composite system a sustainable solution for industrial structures requiring lightweight yet high-performance framing systems.

REFERENCES

- [1] ASCE/SEI 74-23, "Load and Resistance Factor Design (LRFD) for Pultruded Fiber Reinforced Polymer (FRP) Structures," American Society of Civil Engineers: Reston, VA, USA, 2023. <https://doi.org/10.1061/9780784415771>
- [2] Fam, A., Rizkalla, S., "Large scale testing and analysis of hybrid concrete/composite tubes for circular beam-column applications," *Constr. Build. Mater.*, Vol. 17, No. 6–7, pp. 507–516, 2003. [https://doi.org/10.1016/S0950-0618\(03\)00048-5](https://doi.org/10.1016/S0950-0618(03)00048-5)
- [3] Ji, H.S., Song, W., Ma, Z.J., "Design, test and field application of a GFRP corrugated-core sandwich bridge," *Eng. Struct.*, Vol. 32, No. 9, pp. 2814–2824, 2010. <https://doi.org/10.1016/j.engstruct.2010.05.001>
- [4] Ascione, L., Berardi, V.P., Giordano, A., Spadea, S., "Buckling failure modes of FRP thin-walled beams," *Compos. B Eng.*, Vol. 47, pp. 357–364, 2013. <https://doi.org/10.1016/j.compositesb.2012.11.006>
- [5] Jawdhari, A., Fam, A., Nođ, M., "Design equation for concrete-filled FRP tubes in flexure including damage effects," *Eng. Struct.*, Vol. 239, p. 112267, 2021. <https://doi.org/10.1016/j.engstruct.2021.112267>
- [6] Li, Z., Khennane, A., Hazell, P.J., Remennikov, A.M., "Performance of a hybrid GFRP-concrete beam subject to low-velocity impacts," *Compos. Struct.*, Vol. 206, pp. 425–438, 2018. <https://doi.org/10.1016/j.compstruct.2018.08.036>
- [7] Bakis, CE., Bank, LC., Brown, VL., Cosenza, E., Davalos, JF., Lesko, JJ., "Fiber reinforced polymer composites for construction-state-of-the-art review," *ASCE J Compos Constr.*, Vol. 6, No. 2, pp. 73–87, 2002. [https://doi.org/10.1061/\(ASCE\)1090-0268\(2002\)6:2\(73\)](https://doi.org/10.1061/(ASCE)1090-0268(2002)6:2(73))
- [8] Hollaway, LC., "The evolution of and the way forward for advanced polymer composites in the civil infrastructure," *Constr Build Mater.*, Vol. 17, No. 6–7, pp. 365–78, 2003. [https://doi.org/10.1016/S0950-0618\(03\)00038-2](https://doi.org/10.1016/S0950-0618(03)00038-2)
- [9] Einde, LVD., Zhao, L., Seible, F., "Use of FRP composites

- in civil structural applications," *Constr Build Mater.* Vol. 17, No. 6–7, pp. 389–403, 2003. [https://doi.org/10.1016/S0950-0618\(03\)00040-0](https://doi.org/10.1016/S0950-0618(03)00040-0)
- [10] Bank, LC., Gentry, TR., "Development of a pultruded composite material highway guardrail," *Compos Part A*; Vol. 32, No. 9, pp. 1329–38, 2001. [https://doi.org/10.1016/S1359-835X\(01\)00086-0](https://doi.org/10.1016/S1359-835X(01)00086-0)
- [11] Karbhari, VM., "Fiber reinforced composite bridge systems-transition from the laboratory to the field," *Compos Struct*, Vol. 66, No. 1–4, pp. 5–16, 2004. <https://doi.org/10.1016/j.compstruct.2004.04.026>
- [12] Hyeong-Yeol Kim, Ki-Tae Park, Jinwoo Jeong, Young-Ho Lee, Yoon Koog Hwang, Dohak Kim, "A pultruded GFRP deck panel for temporary structures," *Composite Structures*, Vol. 91, No. 1, pp. 20–30, 2009. <https://doi.org/10.1016/j.compstruct.2009.04.028>
- [13] Correia, J. R., Branco, F. A., & Ferreira, J. G., "Flexural behaviour of GFRP–concrete hybrid beams with interconnection slip," *Composite Structures*, Vol. 77, No. 1, pp. 66–78, 2007. <https://doi.org/10.1016/j.compstruct.2005.06.003>
- [14] Abdalla H, "Evaluation of deflection in concrete members reinforced with fibre reinforced polymer (FRP) bars," *Compos Struct*, Vol. 56, No. 1, pp. 63–71, 2002. [https://doi.org/10.1016/S0263-8223\(01\)00188-X](https://doi.org/10.1016/S0263-8223(01)00188-X)
- [15] Ferdous W, Manalo A, Aravinthan T, "Effect of beam orientation on the static behaviour of phenolic core sandwich composites with different shear span-to-depth ratios," *Compos Struct*, Vol. 168, pp. 292–304, 2017. <https://doi.org/10.1016/j.compstruct.2017.02.061>
- [16] Manalo AC, "Behaviour of fibre composite sandwich structures under short and asymmetrical beam shear tests," *Compos Struct*, Vol. 99, pp. 339–49, 2013. <https://doi.org/10.1016/j.compstruct.2012.12.010>
- [17] Bouguerra K, Ahmed E, El-Gamal S, Benmokrane B, "Testing of full-scale concrete bridge deck slabs reinforced with fiber-reinforced polymer (FRP) bars," *Constr Build Mater*, Vol. 25, No. 10, pp. 3956–65, 2011. <https://doi.org/10.1016/j.conbuildmat.2011.04.028>
- [18] Maranan G, Manalo A, Benmokrane B, Karunasena W, Mendis P, "Evaluation of the flexural strength and serviceability of geopolymer concrete beams reinforced with glass-fibre-reinforced polymer (GFRP) bars," *Eng Struct*, Vol. 101, pp. 529–41, 2015. <https://doi.org/10.1016/j.engstruct.2015.08.003>
- [19] Maranan G, Manalo A, Benmokrane B, Karunasena W, Mendis P, "Behavior of con-centrally loaded geopolymer-concrete circular columns reinforced longitudinally and transversely with GFRP bars," *Eng Struct*, Vol. 117, pp. 422–36, 2016. <https://doi.org/10.1016/j.engstruct.2016.03.036>
- [20] Z. Cao, L. Shen, J. Zhao, et al., "Modeling the dynamic mechanism between cement CO₂ emissions and clinker quality to realize low-carbon cement," *Resour. Conserv. Recycl.*, Vol. 113, pp. 116–126, 2016. <https://doi.org/10.1016/j.resconrec.2016.06.011>
- [21] J.L. Vizca ño, S.S. Berriel, S.D. Carrera, et al., "Industrial trial to produce a low clinker, low carbon cement," *Mater. Constr.* Vol. 65, No. 317, 2015. <https://doi.org/10.3989/mc.2015.00614>
- [22] A. Maldonado-Alameda, A.M. Lacasta, J. Giro-Paloma, et al., "Magnesium phosphate cements formulated with low grade magnesium oxide incorporating phase change materials for thermal energy storage," *Constr. Build. Mater.* Vol. 155, pp. 209–216, 2017. <https://doi.org/10.1016/j.conbuildmat.2017.07.227>
- [23] L.F. Cabeza, C. Barreneche, L. Mir Oacute, et al., "Low carbon and low embodied energy materials in buildings: a review," *Renew. Sustain. Energy Rev.* Vol. 23, pp. 536–542, 2013. <https://doi.org/10.1016/j.rser.2013.03.017>
- [24] W.A. Klemm, R.L. Berger, "Accelerated curing of cementitious systems by carbon dioxide: Part I. Portland cement," *Cem. Concr. Res.* Vol. 2, No. 5, pp. 567–576, 1972. [https://doi.org/10.1016/0008-8846\(72\)90111-1](https://doi.org/10.1016/0008-8846(72)90111-1)
- [25] S. Ahmad, R.A. Assaggaf, M. Maslehuddin, et al., "Effects of carbonation pressure and duration on strength evolution of concrete subjected to accelerated carbonation curing," *Constr. Build. Mater.* Vol. 136, pp. 565–573, 2017. <https://doi.org/10.1016/j.conbuildmat.2017.01.069>
- [26] X. Pan, C. Shi, X. Hu, et al., "Effects of CO₂ surface treatment on strength and permeability of one-day-aged cement mortar," *Constr. Build. Mater.* Vol. 154, pp. 1087–1095, 2017. <https://doi.org/10.1016/j.conbuildmat.2017.07.216>
- [27] S. Monkman, Y. Shao, "Carbonation curing of slag-cement concrete for binding CO₂ and improving performance," *J. Mater. Civ. Eng.* Vol. 22, No. 4, pp. 296–304, 2010. [https://doi.org/10.1061/\(ASCE\)MT.1943-5533.0000018](https://doi.org/10.1061/(ASCE)MT.1943-5533.0000018)
- [28] Yuli Wang, Fengxia He, Lei Yang, "Influence of dry ice on the performance of Portland cement and its mechanism," *Construction and Building Materials*, Vol. 188, pp. 898–904, 2018. <https://doi.org/10.1016/j.conbuildmat.2018.08.109>
- [29] Faris Matalkah, Parviz Soroushian, "CO₂ treatment of ground granulated blast furnace slag for enhancing geopolymer properties," *Journal of Materials Research and Technology*, Vol. 17, pp. 2457–2465, 2022. <https://doi.org/10.1016/j.jmrt.2022.01.161>
- [30] Yamgar, S., Takkalaki, S., "Study and Analysis of Strength of GGBS Concrete," *International Journal of Engineering and Management Research*, Vol. 8, No. 6, pp. 28–47, 2018. <https://doi.org/10.31033/ijemr.8.6.4>
- [31] Ali Phul, A., Memon, M., Shah, S., Sandhu, A., "GGBS And Fly Ash Effects on Compressive Strength by Partial Replacement of Cement Concrete," *Civil Engineering Journal*, Vol. 5, No. 4, pp. 913–921, 2019. <https://doi.org/10.28991/cej-2019-03091299>
- [32] Anas, and Afaque Khan, M., "A Review on Ground Granulated Blast-Furnace Slag as a Cement replacing material," *International Research Journal of Engineering and Technology*, Vol. 5, No. 4, pp. 4526–4531, 2018. [Online]. Available: <https://www.irjet.net/archives/V5/i4/IRJET-V5I41007.pdf>
- [33] Kumar Karri, S., Rao, G., and Raju, P., "Strength and Durability Studies on GGBS Concrete," *SSRG International Journal of Civil Engineering*, Vol. 2, No. 10, pp. 34–41, 2015. <https://doi.org/10.14445/23488352/IJCE-V2I10P106>

- [34] K. M. K. and Ketema, E., "Ground Granulated Blast Furnace Slag is used as Concrete Material in Construction," *International Journal for Research in Applied Science & Engineering Technology*, Vol. 7, No. 6, pp. 486–490, 2019. <http://doi.org/10.22214/ijraset.2019.6086>
- [35] Suvarna, A., Salunke, P., Gore, P., and Narkehde, P., "Silica Fume & Ground Granulated Blast Furnace Slag as Cement Replacement in Fiber Reinforced Concrete," *International Research Journal of Engineering and Technology*, Vol. 2, No. 7, pp. 438–443, 2015. [Online]. Available: <https://www.irjet.net/archives/V2/i7/IRJET-V2I767.pdf>
- [36] Acıkök, F., Canpolat, O., Uysal, M., Aygörmez, Y., and Şahin, F., "Effect of Fly Ash and Ground Granulated Blast Furnace Slag on The Strength of Concrete Pavement," *Journal of Sustainable Construction Materials and Technologies*, Vol. 3, No. 3, pp. 278–285, 2018. <https://doi.org/10.29187/jscmt.2018.31>
- [37] Yamgar, S., and Takkalaki, S., "Study and Analysis of Strength of GGBS Concrete," *International Journal of Engineering and Management Research*, Vol. 8, No. 6, pp. 28–47, 2018. <https://doi.org/10.31033/ijemr.8.6.4>
- [38] D. Suresh and K. Nagaraju, "Ground granulated blast slag (GGBS) in concrete—a review," *IOSR Journal of Mechanical and Civil Engineering*, Vol. 12, No. 4, pp. 76–82, 2015. <https://doi.org/10.9790/1684-12467682>
- [39] Desta Shumuye, E., & Jun, Z., "A Review on Ground Granulated Blast Slag (GGBS) in Concrete," *Proc. Of the Eighth International Conference on Advances in Civil and Structural Engineering*, 2018. <https://doi.org/10.15224/978-1-63248-145-0-14>
- [40] Pandey, R., Kumar, A., and Khan, M., "Effect of Ground Granulated Blast Furnace Slag as Partial Cement Replacement on Strength and Durability of Concrete: A Review," *International Research Journal of Engineering and Technology*, Vol. 3, No. 2, pp. 1662–1666, 2014. <https://www.irjet.net/archives/V3/i2/IRJET-V3I2296.pdf>
- [41] Divsholi, B., Lim, T., and Teng, S., "Durability Properties and Microstructure of Ground Granulated Blast Furnace Slag Cement Concrete," *International Journal of Concrete Structures and Materials*, Vol. 8, No. 2, pp. 157–164, 2014. <https://doi.org/10.1007/s40069-013-0063-y>
- [42] Ayub, T., Khan, S., and Memon, F., "Mechanical Characteristics of Hardened Concrete with Different Mineral Admixtures: A Review," *The Scientific World Journal*, Vol. 2014, No. 1, p. 875082, 2014. <https://doi.org/10.1155/2014/875082>
- [43] L.G. Li, J.Y. Zheng, J. Zhu, A.K.H. Kwan, "Combined usage of micro-silica and nano-silica in concrete: SP demand, cementing efficiencies and synergistic effect," *Construction and Building Materials*, Vol. 168, pp. 622–632, 2018. <https://doi.org/10.1016/j.conbuildmat.2018.02.181>
- [44] M. Muttashar, A. Manalo, W. Karunasena, W. Lokuge, "Influence of infill concrete strength on the flexural behaviour of pultruded GFRP square beams," *Composite Structures*, Vol. 145, pp. 58–67, 2016. <https://doi.org/10.1016/j.compstruct.2016.02.071>